Supplementary Information

Electron-Beam Induced Transformation of Layered Tin Dichalcogenides

E. Sutter,[1,*] Y. Huang,[2] H.-P. Komsa,[3] M. Ghorbani-Asl,[4] A.V. Krasheninnikov,[3,4] and P. Sutter[5,*]

[1]Department of Mechanical and Materials Engineering, University of Nebraska-Lincoln, Lincoln, NE 68588, USA

[2]Center for Functional Nanomaterials, Brookhaven National Laboratory, Upton, NY 11973, USA

[3]Department of Applied Physics, Aalto University, P.O. Box 11100, FI-00076 Aalto, Finland

[4]Institute of Ion Beam Physics and Materials Research, Helmholtz-Zentrum Dresden-Rossendorf, 01314 Dresden, Germany

[5]Department of Electrical and Computer Engineering, University of Nebraska-Lincoln, Lincoln, NE 68588, USA

Contents:

1. Supplementary Figures
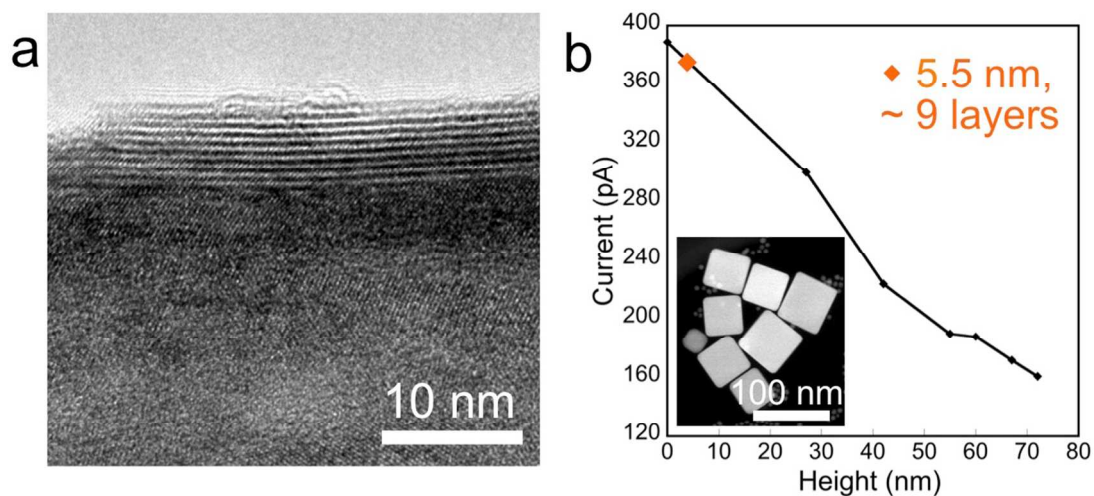
Figure S1. Thickness determination for few-layer SnSe$_2$. (a) Cross-sectional TEM along the folded edge of the SnSe$_2$ flake, showing the layered structure with 9 atomic layers. The measured interlayer spacing is 0.62 nm. **(b)** Beam-current attenuation measured on Ag cubes with different sizes (line and black symbols) and the 9 layer thick SnSe$_2$ flake shown in (a) (orange diamond). The measurements show a similar thickness-dependent electron-beam attenuation for Ag and SnSe$_2$.
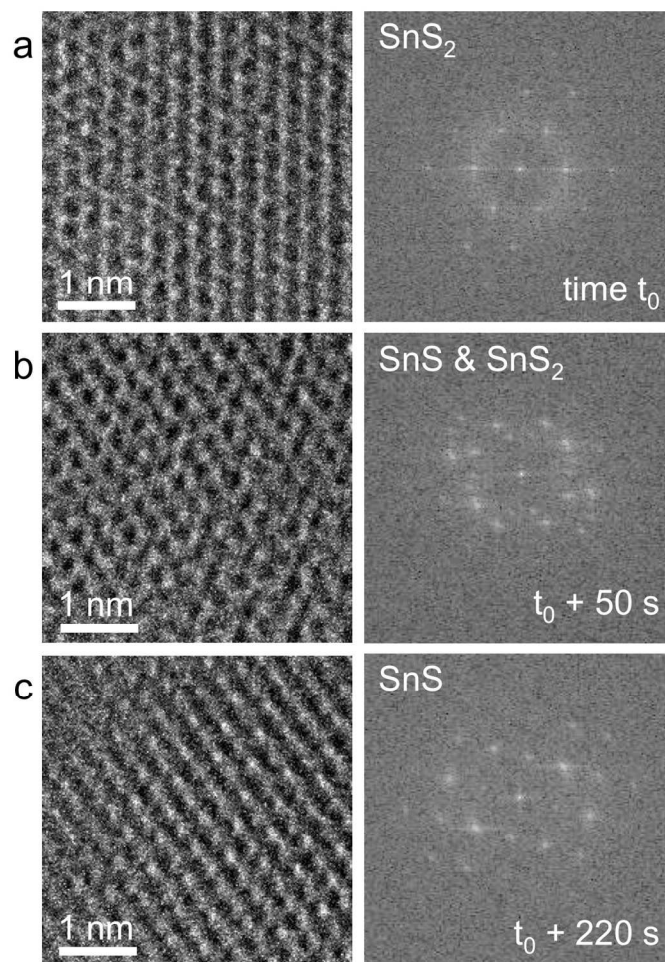
**Figure S2. SnS$_2$ flake evolution under electron beam irradiation at room temperature. (a)** TEM image of small area from the flake followed in Movie M2 and the corresponding power spectrum of the image showing the SnS$_2$ crystal structure at the initiation of the observations. **(b)** TEM image and the corresponding power spectrum of the same area after 50 seconds. The power spectrum shows a superposition of the original SnS$_2$ reflections and additional reflections that can be indexed to the orthorhombic α-SnS crystal structure. **(c)** TEM image and the corresponding power spectrum of the thin flake after 220 seconds. The power spectrum can be indexed to [011]-oriented orthorhombic α-SnS crystal.
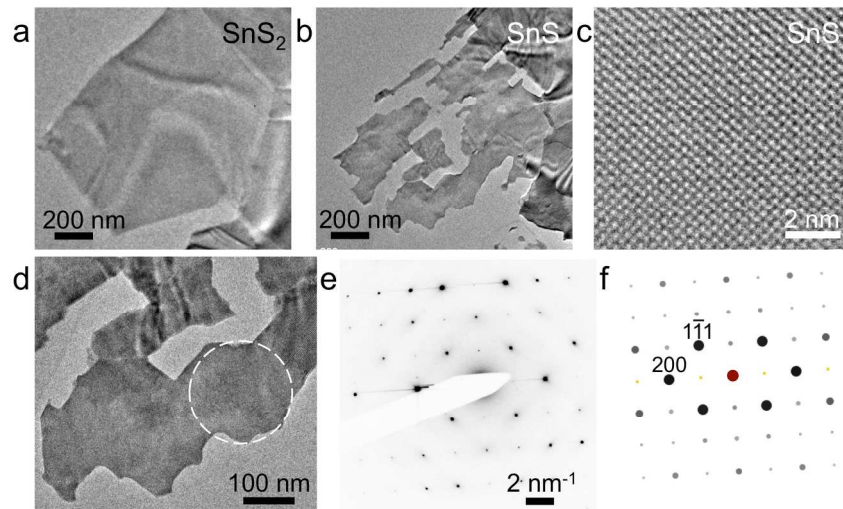
Figure S3. Transformation from SnS$_2$ to SnS at elevated temperature (400°C). a. Few-layer SnS$_2$ flake. **b.** Same flake after electron irradiation at 400°C. **c.** HR-TEM image of the transformed layered crystal. **d.** Higher magnification view of a portion of the SnS flake. **e.** Electron diffraction pattern obtained in the marked region in d. **f.** Calculated diffraction pattern of SnS along the [011] zone axis.
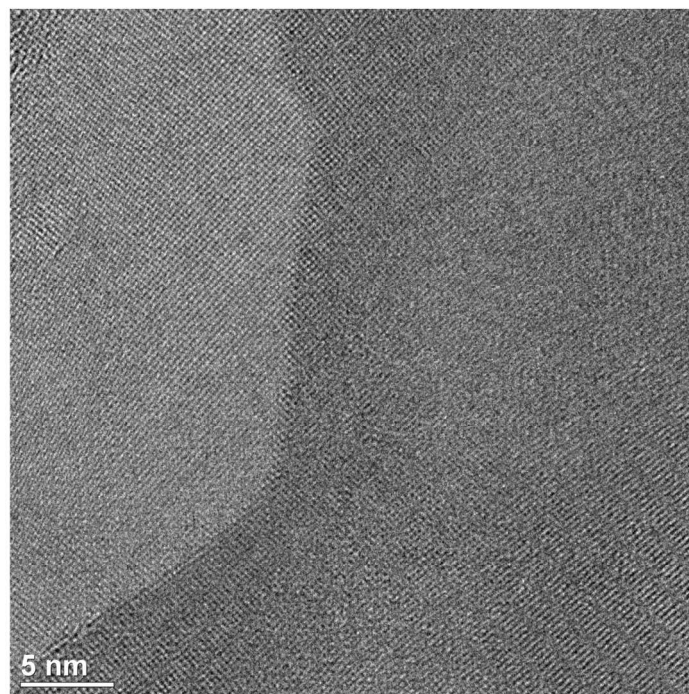
Figure S4. Thinning and structural transformation of a SnS$_2$ flake at 400°C. Extended in-plane faceting of the steps between thick and thin sections of the flake, with the thin area assuming a hexagonal shape, is clearly visible.
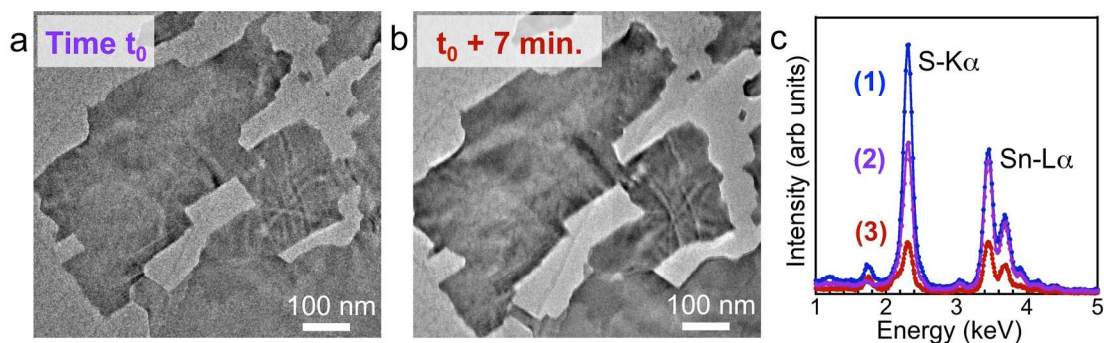
Figure S5. Extended electron-beam exposure at 400°C. (a) SnS flake transformed from SnS$_2$ by electron-beam exposure at 400°C. **(b)** Same area after additional 7 min. exposure. **(c)** Time-dependent EDS spectra, showing the transformation from SnS$_2$ (1) to SnS (2) indicated by a change in the Sn-Lα:S-Kα intensity ratio followed by a uniform reduction of the Sn-Lα and S-Kα intensity (3), accompanying the thinning of the SnS flake with unchanged composition.
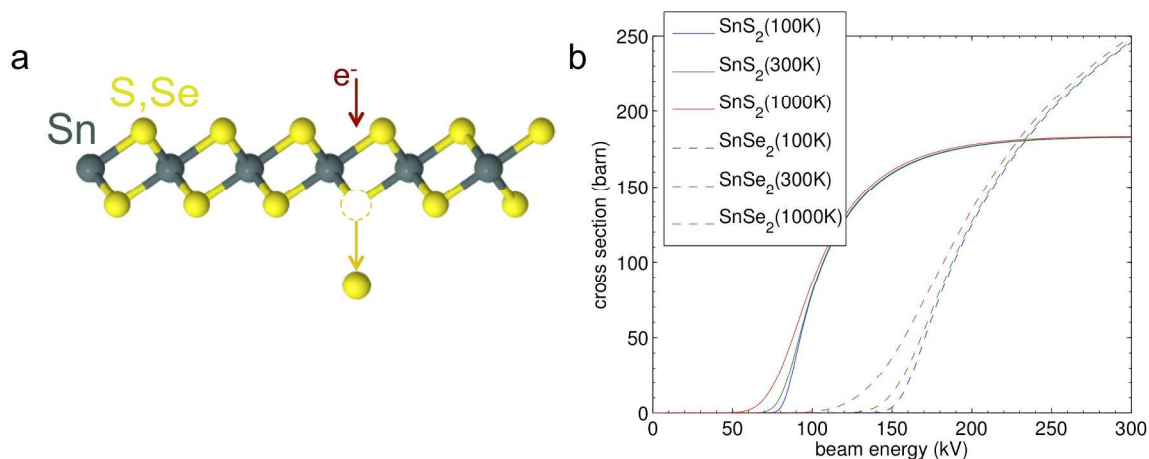

Figure S6. (a) Schematic representation of the knock-on sputtering of S (Se) atoms from a single layer of SnS$_2$ (SnSe$_2$). **(b)** Cross-section for sputtering of a sulfur (selenium) atom from SnS$_2$ (SnSe$_2$) sheets as calculated through the McKinley-Feshbach formalism.
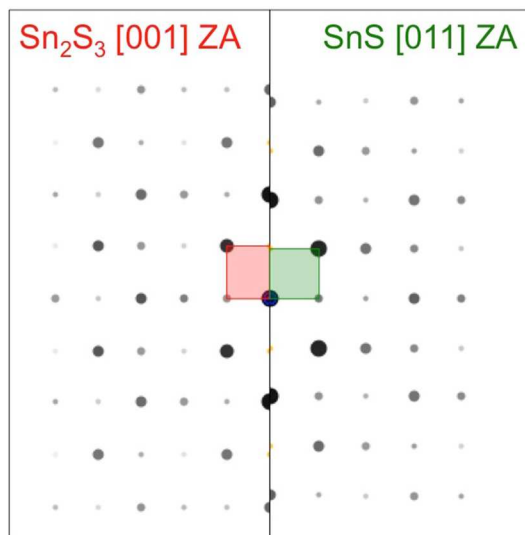
Figure S7. Comparison of the calculated electron diffraction patterns of Sn_2S_3 (along [001] ZA) and tilted SnS (along [011] ZA), showing the same symmetry but small differences in the reciprocal space unit cells.
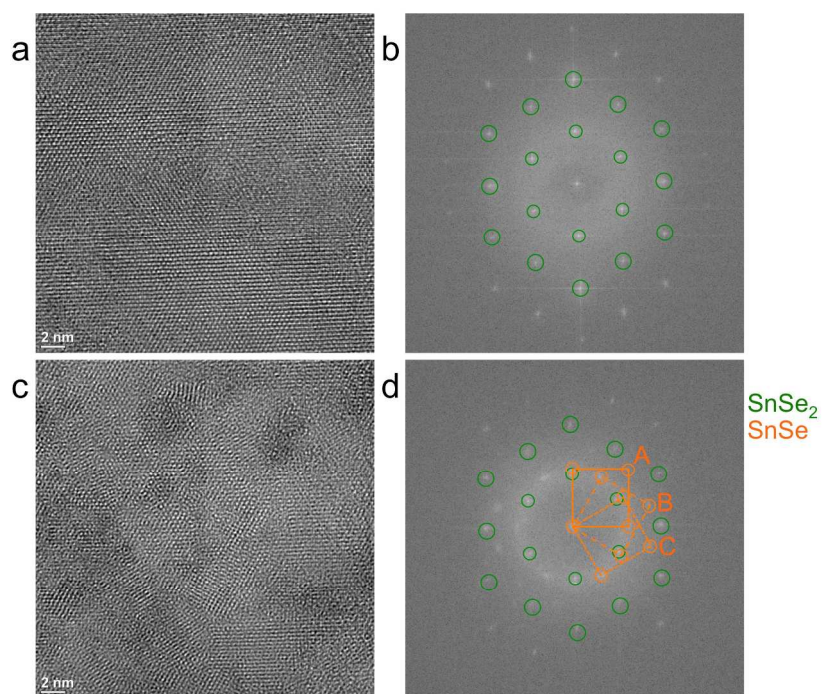
Figure S8. SnSe$_2$ flake evolution under electron beam irradiation at room temperature. (a) TEM image of a thin area from one of the flakes. **(b)** Power spectrum showing the crystal structure of c-axis oriented SnSe$_2$. **(c)** TEM image of the thin flake after electron-beam exposure. **(d)** Power spectrum showing a superposition of the original SnSe$_2$ spots and additional reflections that can be indexed to three distinct orientations (A, B, C) of orthorhombic, c-axis oriented SnSe.
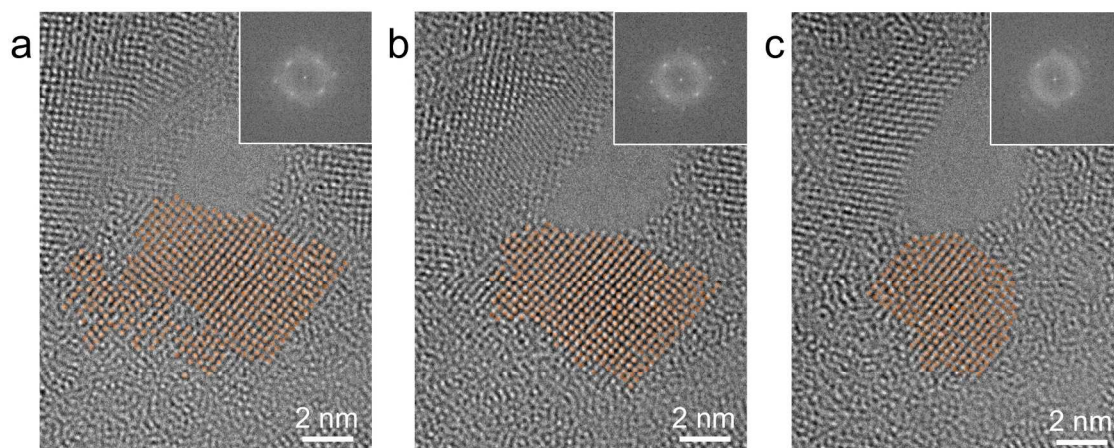
Figure S9. (001) SnSe flake evolution under electron beam irradiation at room temperature.
(a) TEM image of a thin area showing a SnSe flake: marked in the image. The lattice spacing and the power spectrum in the inset confirm the (001) plane of SnSe. **(b)** TEM image of the same area after 54 s of electron-beam exposure. The size of the flake has decreased. The power spectrum in the inset shows that the flake has higher crystalline order than in a. **(c)** Image of the same flake after additional 180 s, showing a significant decrease in the size and more disordered arrangement of the atoms in the flake.
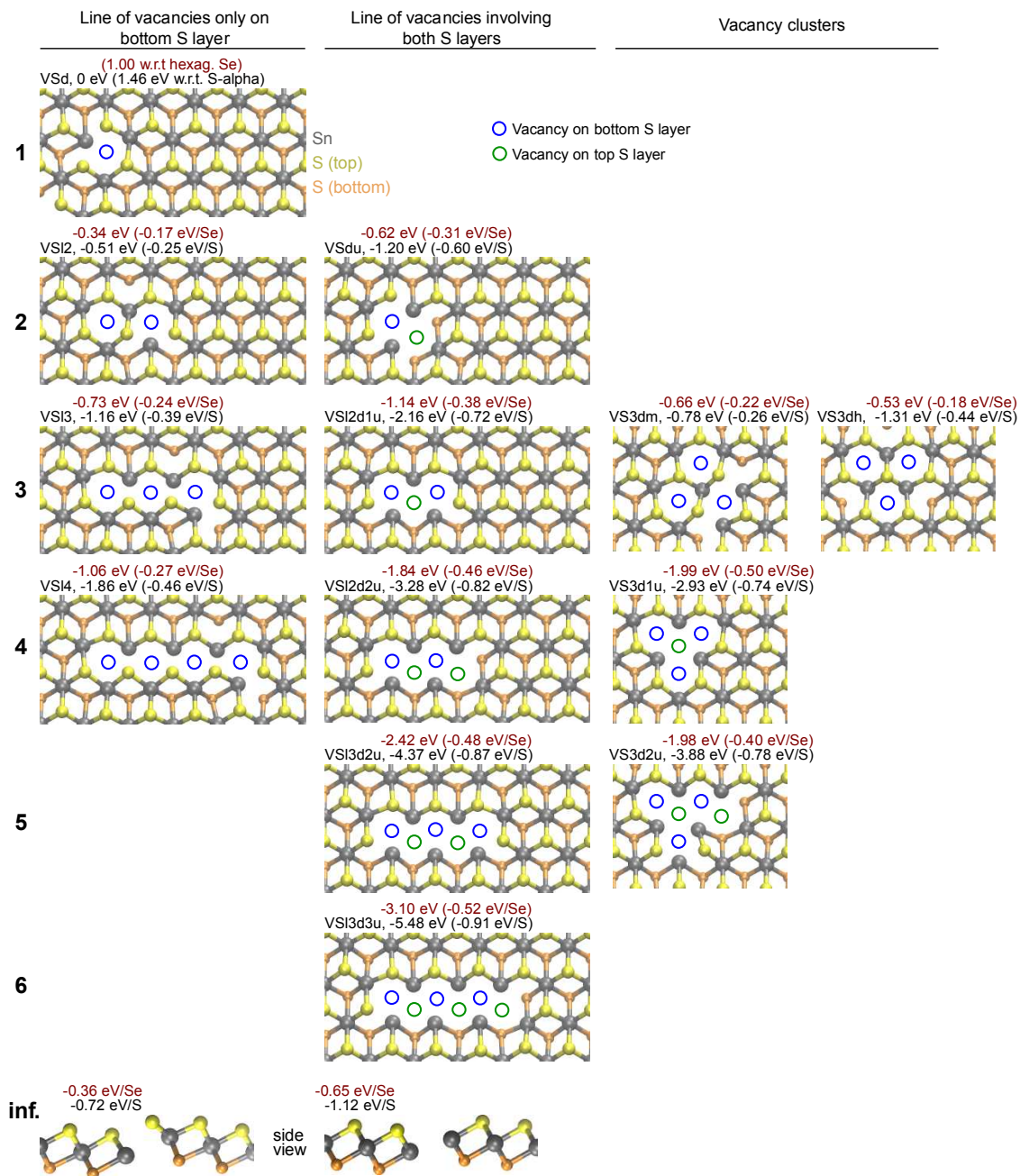
Figure S10. Formation energies and atomic structures of various vacancy configurations in SnS₂ ordered by the configuration type (columns) and the number of missing S/Se atoms (rows). The energies for SnSe₂ are also given (brown). The formation energies are given with respect to the same number of isolated vacancies (and in parentheses divided by the number of missing S/Se).
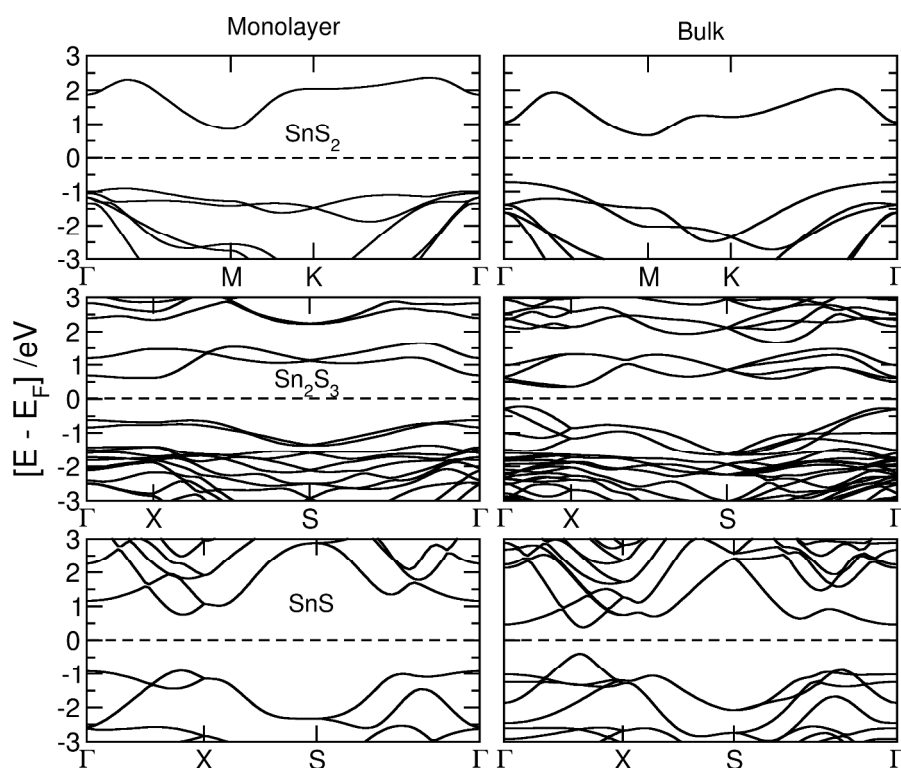
Figure S11. Electronic band structures. Top: SnS$_2$. **Center:** Sn$_2$S$_3$. **Bottom:** SnS. The horizontal dashed lines indicate the Fermi level.
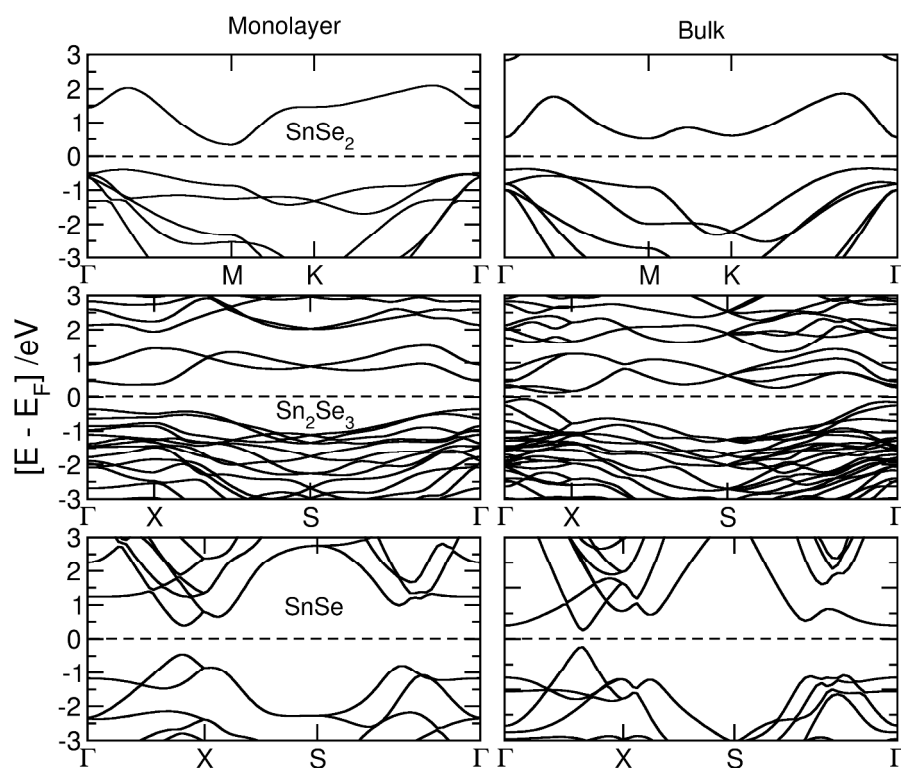
Figure S12. Electronic band structures. Top: SnSe$_2$. **Center:** Sn$_2$Se$_3$. **Bottom:** SnSe. The horizontal dashed lines indicate the Fermi level.
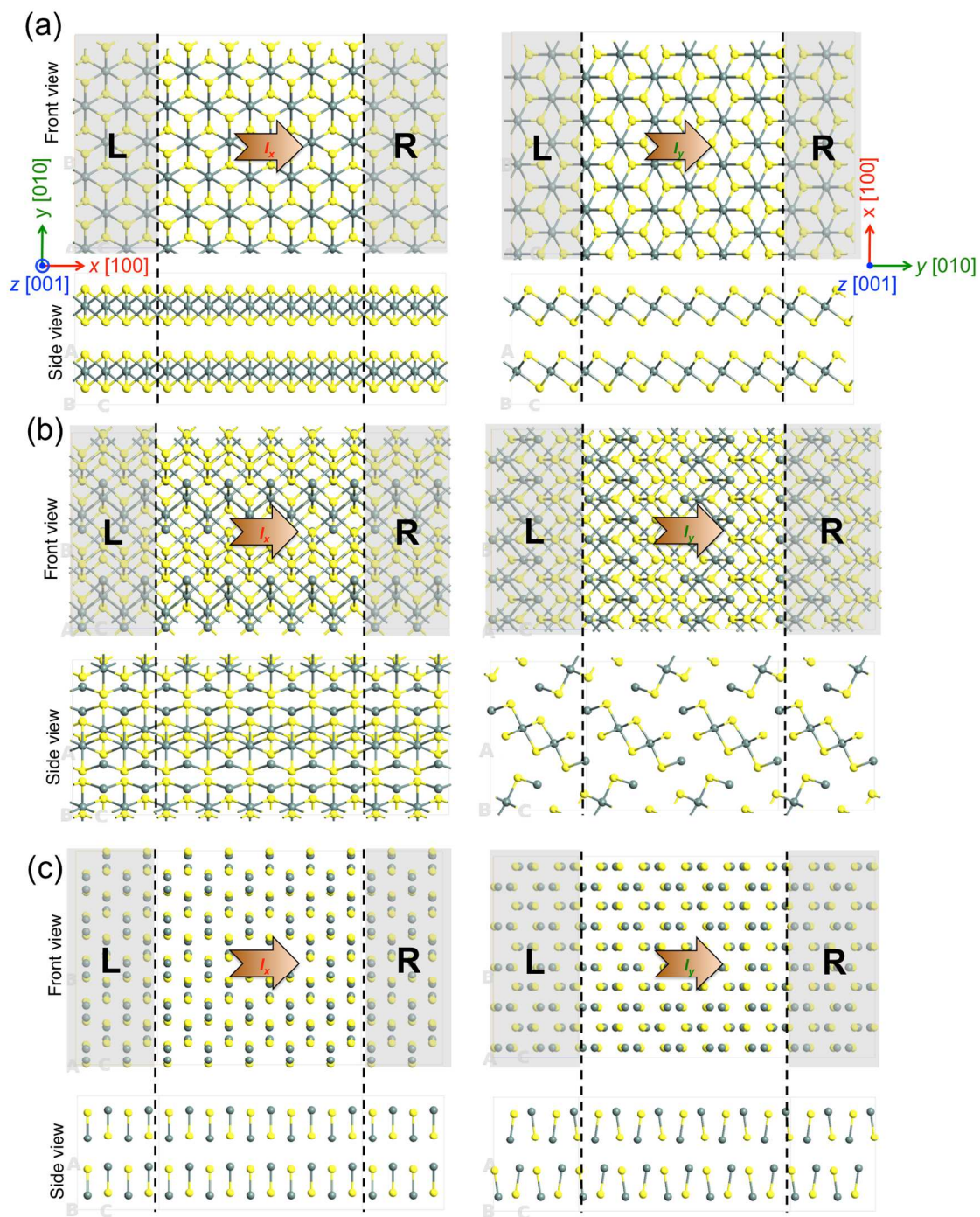
Figure S13. Schematic representation of electronic devices (top and side views). (a) bulk SnS$_2$. **(b)** bulk Sn$_2$S$_3$. **(c)** bulk SnS. The channel region (C) is marked by the dashed lines. The regions labeled "L" and "R" represent the semi-infinite left (source) and right (drain) electrodes. The arrow indicates the transport direction along x ([100]) and y ([010]) in-plane directions.
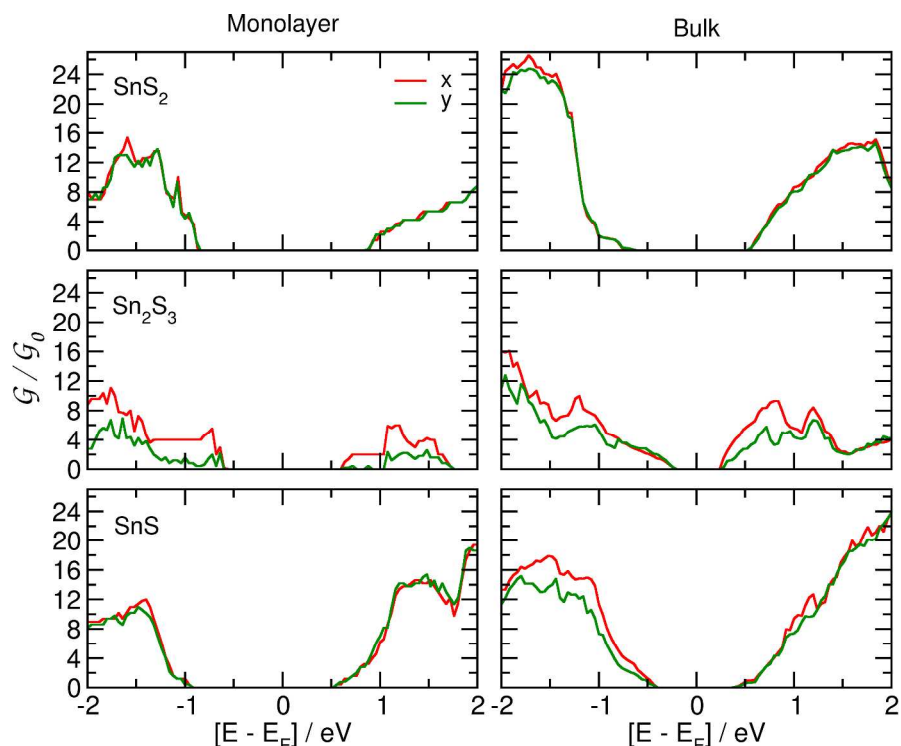
Figure S14. Electrical conductance of Sn-sulfides. Conductance as a function of energy for monolayer and bulk SnS_2, Sn_2S_3 and SnS, along *x* and *y* in-plane directions (see Fig. S13).
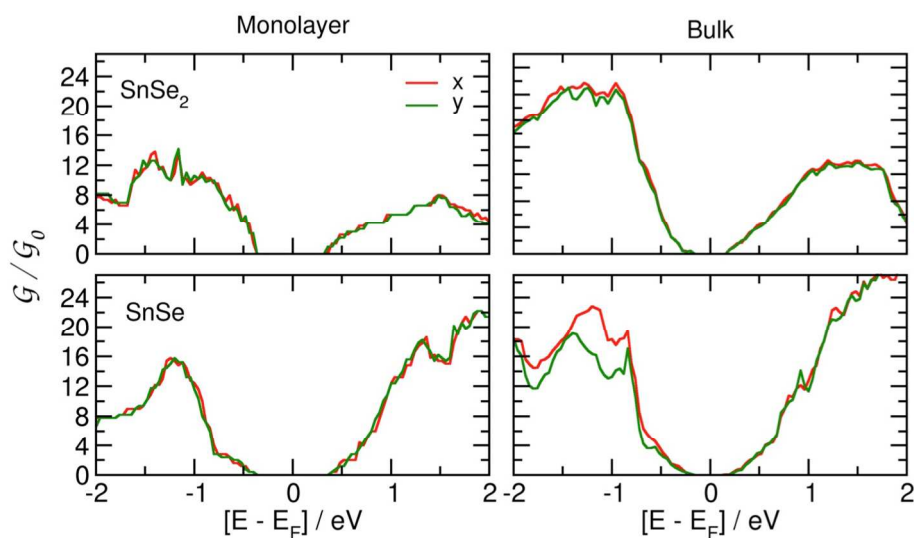
Figure S 15. Electrical conductance of Sn-selenides. Conductance as a function of energy for monolayer and bulk $SnSe_2$ and SnSe, along *x* and *y* in-plane directions.
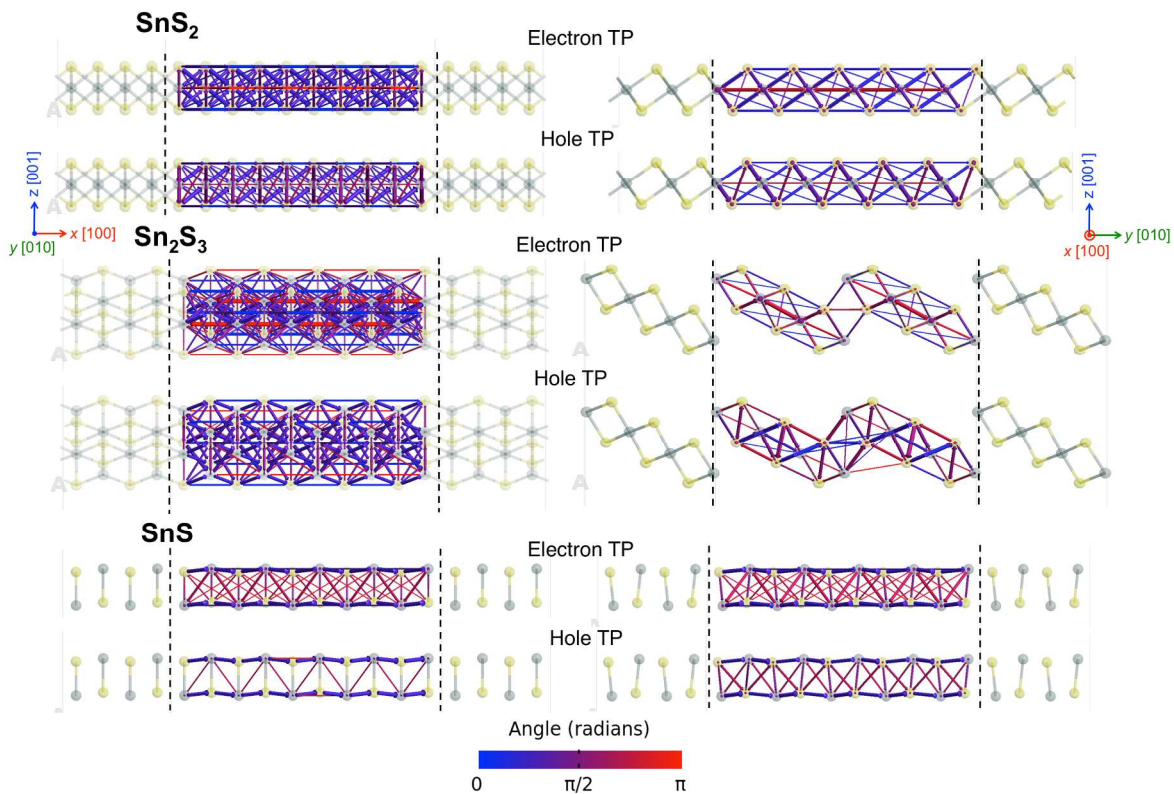
Figure S 16. Electron and hole transmission pathways (TP) for monolayers of SnS$_2$ (top), Sn$_2$S$_3$ (center), and SnS (bottom), along x (left) and _y_ (right) in-plane directions. The transmission peaks in the valence band and conduction band are chosen as the energy values for holes and electrons, respectively. The magnitudes and directions of the transmission pathways are indicated by the thickness and color of the arrows, respectively. The threshold and scale factor are the same for all the plots.

2. Supplementary Tables

Table S1. Formation enthalpy at 0 K and without ZPE for bulk systems. Energies are per formula unit, first line eV, second line kJ/mol, Experimental values (Exp.) in kJ/mol, and $\Delta E = E(Sn_2S_3) - (E(SnS) + E(SnS_2))$.

	SnS	Sn_2S_3	SnS_2	ΔE
LDA	-1.01	-2.34	-1.32	-0.00
	-98	-225	-127	
PBE	-0.82	-1.80	-1.00	0.03
	-80	-173	-96	
PBE-D2	-1.17	-2.54	-1.38	0.01
	-113	-245	-133	
revB86b	-1.10	-2.49	-1.36	-0.02
	-107	-240	-132	
Exp.	-100 to -108	-249 to -297	-148 to -182	< 0
	SnSe	Sn_2Se_3	$SnSe_2$	ΔE
LDA	-0.89	-1.92	-1.05	0.03
	-86	-185	-101	
PBE	-0.89	-1.93	-1.06	0.03
	-86	-186	-102	
PBE-D2	-1.10	-2.29	-1.25	0.05
	-106	-221	-121	
revB86b	-0.98	-2.04	-1.08	0.01
	-94	-197	-104	
Exp.				> 0

Table S2. Lattice parameters for bulk systems (in Å).

	SnS	Sn_2S_3	SnS_2
LDA	10.97, 3.96, 4.16	8.59, 3.76, 13.59	3.63, 5.70
PBE	11.42, 4.02, 4.42	9.27, 3.80, 14.41	3.70, 7.08
PBE-D2	11.38, 4.01, 4.27	8.84, 3.78, 13.98	3.69, 5.89
revB86b	11.28, 4.02, 4.30	8.85, 3.80, 13.96	3.68, 5.88
Expt.	11.32, 4.05, 4.24	8.87, 3.75, 14.02	3.64, 5.89
	SnSe	Sn_2Se_3	$SnSe_2$
LDA	11.31, 4.12, 4.30	8.91, 3.94, 14.16	3.80, 5.90
PBE	11.76, 4.21, 4.55	9.68, 3.99, 14.83	3.87, 8.22
PBE-D2	11.63, 4.20, 4.36	9.19, 3.92, 14.80	3.83, 6.16
revB86b	11.63, 4.20, 4.43	9.22, 3.99, 14.55	3.88, 6.11
Expt.	11.57, 4.19, 4.46		3.81, 6.14

Table S3. Band gaps (in eV) of monolayer and bulk SnS$_2$(Se$_2$), Sn$_2$S$_3$(Se$_3$), SnS(Se) calculated at DFT/PBE+SOC level.

Material	Monolayer	Bulk
SnS$_2$	1.75	1.37
Sn$_2$S$_3$	1.23	0.56
SnS	1.66 (d)*	0.78
SnSe$_2$	0.73	0.88
Sn$_2$Se$_3$	0.70	0.18
SnSe	0.87 (d)*	0.34

*d represents a direct band gap

Table S4. The values of electron effective masses for bulk SnS$_2$, Sn$_2$S$_3$ and SnS. Data obtained from DFT/PBE+SOC band structure calculations.

Material	$m^*_{[100]}/m_0$	$m^*_{[010]}/m_0$	$m^*_{[001]}/m_0$	$m^*_{[110]}/m_0$	$m^*_{[101]}/m_0$	$m^*_{[011]}/m_0$
SnS$_2$	0.544	0.328	1.064	0.717	1.025	0.784
Sn$_2$S$_3$	0.275	1.270	0.710	0.488	0.897	3.452
SnS	0.101	0.195	0.699	0.133	0.177	0.305

3. Supplementary Movies
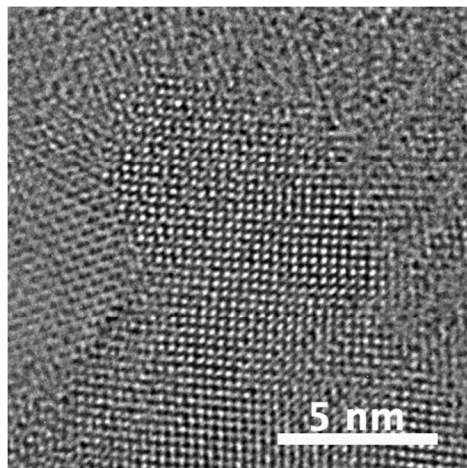
Movie S1: Time-lapse movie of the electron-beam induced transformation of few-layer SnS_2 to SnS at room temperature. Electron energy: 300 keV (FEI Titan 80-300, Orius CCD camera). Total duration: 490 sec. Spatial scale as shown in the movie. 50 frames.
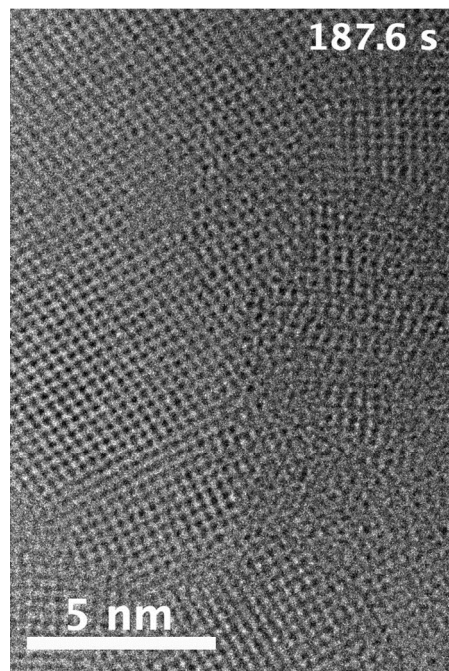
Movie S2: Time-lapse movie of the electron-beam induced transformation of few-layer SnS_2 to SnS at room temperature. Electron energy: 300 keV (FEI Titan 80-300, Gatan K2-IS DDD camera). Actual capture rate: 2.5 milliseconds per frame. The movie shows every 100th frame of the original dataset at 50% scaling. Spatial scale and timing as shown in the movie. 470 frames.

4. Computational details for electronic structure and transport calculations

The electronic structure and quantum transport calculations were performed using Atomistix ToolKit (ATK) code.[1] The calculations have been done using GGA/PBE functional[2] with double-zeta plus polarization numerical basis sets. The effect of spin-orbit coupling (SOC) was considered in all electronic structure calculations. We have used an energy cutoff of 300 Ryd and 0.0002 Ryd of tolerance for the self-consistent calculations. A 9x9x9 and 5×5×100 Monkhorst-Pack k-sampling is used for the electronic structure and transport calculations. A vacuum separation of 30 Å has been applied for simulation of monolayers, which minimizes any artificial interaction between its periodic images. The Poisson-Schrödinger equation of the system was self-consistently solved using a Fast Fourier Transform (FFT) solver. Transport calculations were performed such that the system is divided into three parts: the semi-infinite left (L) and right (R) electrode, and the finite central region (C), also called scattering region. In order to provide straightforward comparison between different orientations, we used a supercell with almost equal length and width along x and y directions for all the calculations. According to the Fisher-Lee formula,[3] the electron conductance at low temperatures can be obtained via transmission matrix (T):

$$\mathcal{G} = \mathcal{G}_0 \sum_n T_n(E) = \mathcal{G}_0 \, Trace\big[\hat{G}_C \hat{\Gamma}_R \hat{G}_C^\dagger \hat{\Gamma}_L\big],$$

where $\mathcal{G}_0$ represents quantum conductance, G_C is the Green's function of the central region and $\hat{\Gamma}_{L,R}$ are the coupling matrices of left and right electrodes.

5. Supplementary References

(1)   QuantumWise A/S. Atomistix ToolKit, 2015, www.quantumwise.com.
(2)   Perdew, J. P.; Burke, K.; Ernzerhof, M. *Phys. Rev. Lett.* **1996**, *77*, 3865–3868.
(3)   Fisher, D. S.; Lee, P. A. *Phys. Rev. B* **1981**, *23*, 6851.